Supplementary Material

A Temporal Model of Cofilin Regulation and the Early Peak of Actin Barbed Ends in Invasive Tumor Cells

Nessy Tania[a], Erin Prosk[a], John Condeelis[b], and Leah Edelstein-Keshet[a1]

[a]Department of Mathematics,
University of British Columbia, Vancouver, BC V6T 1Z2, Canada

[b]Department of Anatomy and Structural Biology,
Gruss Lipper Biophotonics Center,
Albert Einstein College of Medicine of Yeshiva University, Bronx, NY 10461

[1]Corresponding author
Department of Mathematics, University of British Columbia
Room 121, 1984 Mathematics Road, Vancouver, BC V6T 1Z2, Canada.
Phone: 1-604-822-5889. *Fax:* 1-604-822-6074. *Email:* keshet@math.ubc.ca

Contents

1 Nonlinear kinetics of severing

In this section, we explain in detail how we chose the nonlinear function that describes the kinetics of actin filament severing by cofilin (given by Eqn (1) in the main text). This function has to be able to account for how amplification of barbed ends can be produced due to cofilin binding cooperativity. We consider the minimal model in which only the active cofilin level, $C(t)$ and the barbed end density, $B(t)$ are tracked. (Eqs (1,2) in the main text, repeated here for convenience:)

$$\frac{dC}{dt} = \bar{I}_{stim}(t) + I_C - k_p C - F_{sev}(C), \tag{S1}$$

$$\frac{dB}{dt} = I_B - k_{cap} B + \bar{A} F_{sev}(C), \tag{S2}$$

where, I_B and I_C denotes basal rates of production and k_p and k_{cap} the basal rates of degradation and capping. Following a time-dependent stimulus, $\bar{I}_{stim}(t)$, barbed ends are generated when cofilin severs F-actin at the rate $F_{sev}(C)$. F-actin is assumed to be constant and not a limiting factor. The constant $\bar{A}$ in the severing term in the equation for B represents a scale factor for change of units between C, generally given in μM, and the barbed end density, B, is given in units of $\#/\mu\text{m}^2$. A concentration of 1 μM corresponds to approximately 600 molecules/μm^3. For a region of interest (e.g. a lamellipod) of thickness of 0.15 μm, a concentration of 1 μM gives $A = 0.15 \cdot 600 \approx 100$ molecules per 1 μm^2.

When cofilin activity is minimal, we expect the barbed end production rate, $\bar{A} F_{sev}(C)$, to be small. Thus, without stimulation, the rest/steady-state value of B can be approximated by $B^* = I_B/k_{cap}$. To reduce the number of parameters, we scale Eqn. (S2) and consider the non-dimensional quantity $b(t) = B(t)/B^*$ whose dynamics follow

$$\frac{db}{dt} = A f_{sev}(c) + k_{cap}(1 - b). \tag{S3}$$

Eqn. (S1) for C can similarly be scaled by defining $C^* = I_C/k_p$, which results in the following equation for $c(t) = C(t)/C^*$,

$$\frac{dc}{dt} = I_{stim}(t) + k_p(1 - c) - f_{sev}(c). \tag{S4}$$

A, $f_{sev}(c)$ and $I_{stim}(t)$ are the corresponding scaled version of $\bar{A}$, $F_{sev}(C)$, and $\bar{I}_{stim}(t)$ respectively. When $c = 0$, the barbed ends rest level is $b_{ss} = 1$ and amplification is defined as the fold-multiple of this value at the peak or barbed ends, b_{peak}. The definition of the parameters as well as the numerical values used for the non-dimensional model are given in Table S1.

We now study the response of the system when various types of severing functions $f_{sev}(c)$ are used. In all cases, $f_{sev}(c)$ is constructed such that the steady state of the system remains the same. Then, at steady-state, there is very little severing occurring, $f_{sev} = k_{sev}\, c_{ss} << 1$, where c_{ss} is the steady state value of c. Specifically, we consider the following three functions:

(a) A linear severing function,

$$f_{sev}(c) = k_{sev}\, c\,. \tag{S5}$$

Table S1: List of parameters for the minimal model given in Eqs. (S3-S4). Note that parameter values here are chosen to approximately yield the peak of barbed ends seen experimentally (2) and do not reflect the final choice of parameter values used in the detailed cofilin cycle model.

Parameter	Definition	Value
A	scale factor for unit conversions from C to B	$100/\mu\text{m}^2$
k_{cap}	barbed end capping rate	1 /s
k_p	rate of cofilin inactivation/phosphorylation	1 /s
k_{sev}	cofilin mediated severing rate	0.01 /s
n	degree of cooperativity	7

(b) A nonlinear severing function with saturation,

$$f_{sev}(c) = g_{max}\, k_{sev}\, c_{ss} \left(\frac{c^n}{c^n + k_n^n} \right) . \tag{S6}$$

To have $f_{sev} = k_{sev}\, c_{ss}$ at rest, we set $g_{max} = (c_{ss}^n + k_n^n)/c_{ss}^n$. This severing term approximates sequential cooperative binding and the quasi-equilibrium approximation for the following reaction scheme,

$$n \text{ Active Cofilin} + \text{F-actin} \rightarrow \text{Barbed-end} + n \text{ Inactive Cofilin} . \tag{S7}$$

Then, k_n is the dissociation constant for cofilin-actin binding. Other studies have reported that cofilin binds to actin filaments cooperatively as binding changes the structure of the actin filament allowing for further cofilin binding. The binding process can be described by a Hill function of degree 4-10 (1).

(c) A nonlinear severing function with no saturation,

$$f_{sev}(c) = k_{sev}\, c_{ss} \left(\frac{c}{c_{ss}} \right)^n . \tag{S8}$$

This function approximates the behaviour of (S6) for $c \ll k_n$.

To simplify analysis, we set $I_{stim} = 0, b(0) = b_{ss} = 1$ and study the response to various initial levels of $c(0)$ above the normal resting value of $c_{ss} \approx 1$. This represents an initial elevation of cofilin downstream of a stimulus pulse. We then track the change in b relative to its steady-state value. The results are shown in phase-plane plots in Fig. S1. The maximal height of the black curves above $b_{ss} = 1$ in the cb plane can be interpreted as the amplification of barbed ends, i.e., as b_{peak}/b_{ss}. We can thus compare the amplification obtained with a variety of assumptions about the severing kinetics.

For a linear severing function, the degree of barbed-end amplification is weak. For example, increasing cofilin five-fold only results in amplification by a factor of about 2

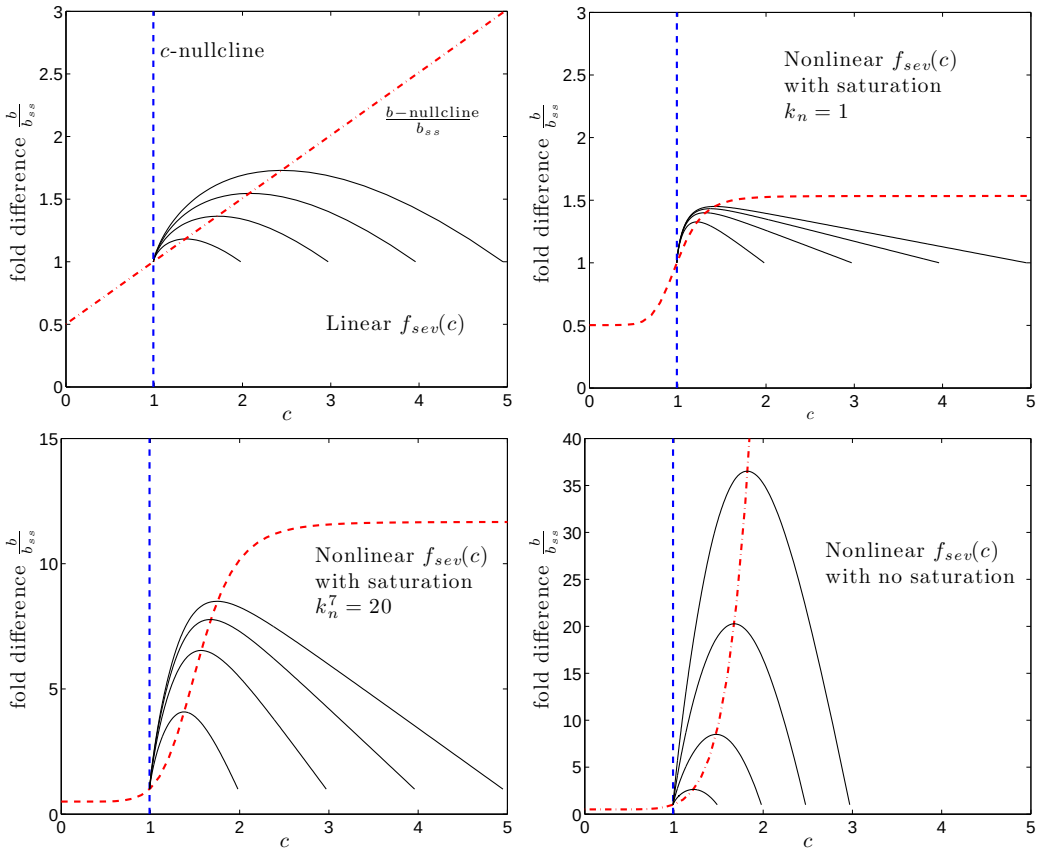

Figure S1: Phase plane behavior of cofilin and barbed end amplification in the two-variable system with severing functions $f_{sev}(c)$ (a-c). Dashed lines indicate nullclines of Eqs. (S3-S4), and solid lines are sample trajectories starting from various elevated levels of cofilin. Amplification is the difference between the maximal height of the black curves and the steady state barbed ends level $b_{ss} = 1$.

($b_{peak} \approx 2b_{ss}$). We can also determine the amount of amplification by treating cofilin, c as a parameter. As c is varied, the "steady-state" level of b is given by

$$b^* = \frac{A f_{sev}(c) + k_{cap}}{k_{cap}}\,. \tag{S9}$$

(This equation also corresponds to the b-nullcline of the full system). If $f_{sev}(c)$ is linear, then changing c by two-fold will at most leads to the doubling of b^*. Thus, to have a large degree of amplification, as observed experimentally, a non-linear severing rate is required. For a Hill function, $f_{sev}(c)$ (Eqn. (S6)), the maximum barbed-end amplification is determined by the saturated level, ($g_{max}\, k_{sev}\, c_{ss}$). Larger degree of amplification is observed as k_n is increased. In the limit of k_n very large relative to the range of c, the severing function no longer saturates and is exactly given by Eqn. (S8) (this is the range far from saturation). This explains our choice of (S8) for the severing function f_{sev} in the models.

2 One-Compartment Cofilin Dynamics Model

We here briefly present the one-compartment model, schematically shown in Fig S2. This model is the first correction of the mini-model presented in the previous section. Here, the cofilin activity cycle, modulated by PIP_2 binding, actin binding, and phosphorylation are taken into account. The equations describing the single compartment model are listed below, and simulation results are later compared with the more detailed two-compartment model using a scaled (dimensionless) model formulation.

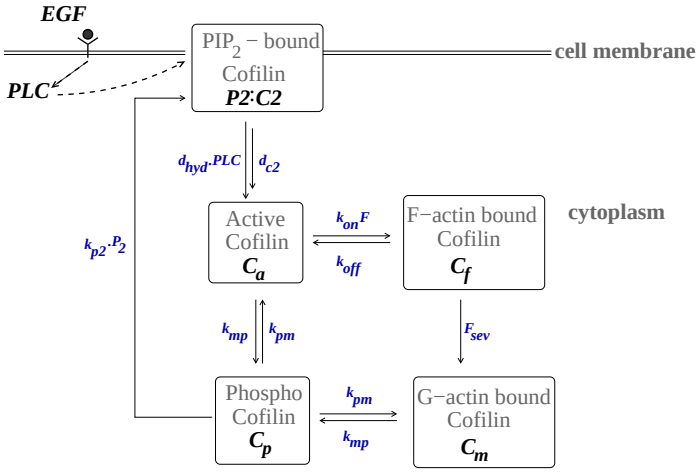

Figure S2: Schematics of the single compartment ODE model for cofilin regulation. Here, the cell is assumed to consist only of one single well-mixed compartment. C_2 is the cofilin fraction bound to PIP_2 on the membrane, C_a is active cofilin in the cytosol, C_f is the fraction bound to F-actin, C_m reflects G-actin-monomer bound cofilin, and C_p is phosphorylated/inactive cofilin.

Equations for the One-Compartment Model

PLC Activity

$$\frac{dPLC}{dt} = \bar{I}_{stim}(t) + I_{plc} - d_{plc}PLC\,, \tag{S10}$$

with the EGF stimulation profile

$$\bar{I}_{stim}(t) = \bar{I}_{stim0} \cdot [H(t - t_{on}) - H(t - t_{off})]\,, \tag{S11}$$

where $H(s)$ is the Heaviside function (i.e. unit step function that turns on at $t = 0$).

PIP_2 level

$$\frac{dP_2}{dt} = I_{p_2} - d_{p_2}P_2 - d_{hyd}\left(\frac{PLC - PLC_{rest}}{PLC_{rest}}\right)P_2\,. \tag{S12}$$

PIP_2-bound cofilin

$$\frac{dC_2}{dt} = k'_{p_2}\left(\frac{P_2}{P_{2,rest}}\right)C_p - d_{c_2}C_2 - d_{hyd}\left(\frac{PLC - PLC_{rest}}{PLC_{rest}}\right)C_2\,. \tag{S13}$$

Active cofilin

$$\frac{dC_a}{dt} = d_{c2}C_2 + d_{hyd}\left(\frac{PLC - PLC_{rest}}{PLC_{rest}}\right)C_2 - k'_{on}F\,C_a + k_{off}C_f - k_{mp}C_a + k_{pm}C_p\,. \tag{S14}$$

F-actin-bound cofilin

$$\frac{dC_f}{dt} = k'_{on}F\,C_a - k_{off}C_f - F_{sev}(C_f)\,, \tag{S15}$$

with the severing function

$$F_{sev}(C_f) = k_{sev}\,C_{f,rest}\left(\frac{C_f}{C_{f,rest}}\right)^n\,. \tag{S16}$$

G-actin-bound cofilin

$$\frac{dC_m}{dt} = F_{sev}(C_f) - k_{mp}C_m + k_{pm}C_p\,. \tag{S17}$$

Phosphorylated cofilin

$$\frac{dC_p}{dt} = k_{mp}(C_a + C_m) - 2k_{pm}C_p - k'_{p_2}\left(\frac{P_2}{P_{2,rest}}\right)C_p\,. \tag{S18}$$

Barbed end production

$$\frac{dB}{dt} = \bar{A}F_{sev}(C_F) - k_{cap}B\,, \tag{S19}$$

Parameters for a (dimensionless form of) this model are as shown in Table S4. The notation for the parameters k'_{on} and k'_{p2} is explained in connection with a comparison between the one and the two pool models. (Briefly, to compare the two models, we set $k'_{on} = k_{on}V_E/V_{tot}$ and $k'_{p_2} = k_{p_2}V_E/V_{tot}$ where volumes are explained in the next section.)

3 Two-Compartment Cofilin Dynamics Model

Here we discuss the geometry of the two-compartment model. Fig. S3 shows a magnified view of the inset in Fig. 1 of the main paper. The edge compartments (representing a nascent lamellipod) is approximated as a thin ring (or "washer") of thickness dR and height l. The interior compartment is approximated as a hemisphere of radius R. The compartment volumes and their contact area (for diffusion and exchange) are thus

$$V_I = \frac{2}{3}\pi R^3, \quad V_E = 2\pi Rl \cdot dR, \quad A_{contact} = 2\pi Rl$$

Diffusion between compartments takes place through the surface that separates these, approximated as a cylinder of radius R and height l and area $A_{contact}$.

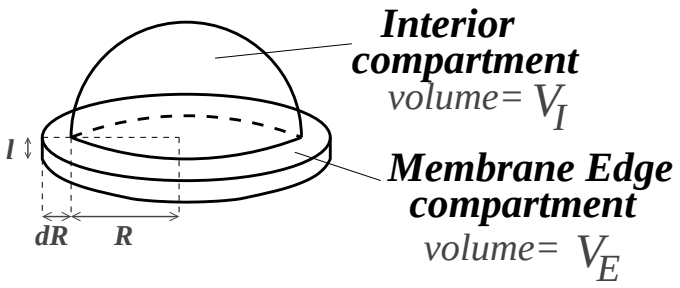

Figure S3: Cell geometry used in the two-compartment model (magnified view of the inset in Fig. 1).

Diffusion Flux Between Compartments

Because compartments are of vastly different sizes, our balance equations contain compartment volume factors to preserve mass conservation. We assume that the cofilin flux between compartments is diffusive, and thus proportional to concentration gradients. Taking into account the distinct volume of the compartments and the area through which diffusive flux takes place, we can write

$$\frac{d(V_E C_i^E)}{dt} = \omega\, D(C_i^I - C_i^E) \pm \text{reaction terms}, \tag{S20}$$

$$\frac{d(V_I C_i^I)}{dt} = -\omega\, D(C_i^I - C_i^E) \pm \text{reaction terms}, \tag{S21}$$

where D is the diffusion coefficient for cofilin (estimated as 10 μm^2/s (3)), and $\omega = 2\pi l$ with l, the thickness of the membrane edge compartment.

The factor ω is obtained as follows. Consider the geometry as in Fig. S3, and suppose C^E, C^I are concentrations of a given cofilin form in the edge and interior compartments. The diffusive flux from the edge to the interior is $J_D = \dfrac{D}{\lambda}(C^I - C^E)$, (number of molecules per unit time per unit area). λ is a typical length scale over which diffusion takes place, assumed to be the cell radius ($\lambda = R + dR \approx R$). The area of contact between the compartments is $A_{contact}$, so the number of molecules crossing this area per unit time is $A_{contact}\, J_D$. We define $\omega = 2\pi l$ and write

$$\frac{d}{dt}(V_E C^E) = (\omega R)\frac{D}{\lambda}(C^I - C^E) + \text{reaction terms} = D(2\pi l)(C^I - C^E) + ... \tag{S22}$$

The above equation is used to track forms of cofilin in the edge compartment that can diffuse between the two compartments. Similar terms occur in several equations in the model displayed below.

Equations for the Two-Compartment Model

PLC Activity

$$\frac{dPLC}{dt} = \bar{I}_{stim}(t) + I_{plc} - d_{plc}PLC\,, \tag{S23}$$

with the EGF stimulation profile

$$\bar{I}_{stim}(t) = \bar{I}_{stim0} \cdot [H(t - t_{on}) - H(t - t_{off})]\,, \tag{S24}$$

where $H(s)$ is the Heaviside function (i.e. unit step function that turns on at $t = 0$).

PIP_2 level

$$\frac{dP_2}{dt} = I_{p_2} - d_{p_2}P_2 - d_{hyd}\left(\frac{PLC - PLC_{rest}}{PLC_{rest}}\right)P_2\,. \tag{S25}$$

PIP_2-bound cofilin

$$\frac{dC_2}{dt} = k_{p_2}\left(\frac{P_2}{P_{2,rest}}\right)C_p^E - d_{c_2}C_2 - d_{hyd}\left(\frac{PLC - PLC_{rest}}{PLC_{rest}}\right)C_2\,. \tag{S26}$$

Active cofilin in the edge compartment

$$\begin{aligned}\frac{dC_a^E}{dt} &= d_{c2}C_2 + d_{hyd}\left(\frac{PLC - PLC_{rest}}{PLC_{rest}}\right)C_2 - k_{on}F\,C_a^E + k_{off}C_f \\ &\quad - k_{mp}C_a^E + k_{pm}C_p^E + \frac{\omega D}{V_E}(C_a^I - C_a^E)\,.\end{aligned} \tag{S27}$$

F-actin-bound cofilin in the edge compartment

$$\frac{dC_f}{dt} = k_{on}F\,C_a^E - k_{off}C_f - F_{sev}(C_f)\,, \tag{S28}$$

with the severing function

$$F_{sev}(C_f) = k_{sev}\,C_{f,rest}\left(\frac{C_f}{C_{f,rest}}\right)^n\,. \tag{S29}$$

G-actin-bound cofilin in the edge compartment

$$\frac{dC_m^E}{dt} = F_{sev}(C_f) - k_{mp}C_m^E + k_{pm}C_p^E + \frac{\omega D}{V_E}(C_m^I - C_m^E)\,. \tag{S30}$$

Phosphorylated cofilin in the edge compartment

$$\frac{dC_p^E}{dt} = k_{mp}(C_a^E + C_m^E) - 2k_{pm}C_p^E - k_{p_2}\left(\frac{P_2}{P_{2,rest}}\right)C_p^E + \frac{\omega D}{V_E}(C_p^I - C_p^E)\,. \tag{S31}$$

Active cofilin in the interior compartment

$$\frac{dC_a^I}{dt} = -k_{mp}C_a^I + k_{pm}C_p^I - \frac{\omega D}{V_I}(C_a^I - C_a^E)\,. \tag{S32}$$

G-actin-bound cofilin in the interior compartment

$$\frac{dC_m^I}{dt} = -k_{mp}C_m^I + k_{pm}C_p^I - \frac{\omega D}{V_I}(C_m^I - C_m^E)\,. \tag{S33}$$

Phosphorylated cofilin in the interior compartment

$$\frac{dC_p^I}{dt} = k_{mp}(C_a^E + C_m^E) - 2k_{pm}C_p^E - \frac{\omega D}{V_I}(C_p^I - C_p^E)\,. \tag{S34}$$

$$\tag{S35}$$

Barbed end production

$$\frac{dB}{dt} = \bar{A}F_{sev}(C_F) - k_{cap}B\,. \tag{S36}$$

Parameters are defined in Table 1 of the main text.

4 Determination of Parameter Values

Parameter Determination from Steady State Constraints

Several rate constants are obtained by imposing the steady state constraints (given in Eqn. (6)). Setting the left hand sides of Eqn. (7-17) to zero, the rate can be obtained by solving a nonlinear system of algebraic equations. We list the formulae obtained in Table S2. Note, however, that although algebraic expressions can be found, some of the rate constants also depend on the steady-state level of various cofilin forms. In many cases, no closed form expressions are possible, and parameters have to be found numerically. We list the steady-state values in Table S3.

Table S2: Parameter values for the two-pool model obtained by setting the steady-state fractions equal to R_i as given in Eqn. (10).

Parameter	Definition	Formula	Value
k_{p2}	binding rate C_p to PIP_2	$d_{c2}\dfrac{R2}{c^E_{p,ss}\cdot v_E}$	0.112/s
k_{pm}	dephosphorylation rate	$\dfrac{k_{mp}(Ra+Rm)-d_{c2}R_2}{2R_p}$	0.03/s
k_{sev}	severing rate	$\dfrac{k_{mp}R_m - k_{pm}R_p}{R_f}$	0.0012/s
$k_{on}F$	rate binding to F-actin	$\dfrac{R_f}{c^E_{a,ss}\cdot v_E}(k_{off}+k_{sev})$	0.198/s

Table S3: The steady-state concentrations for cofilin forms in the two-compartment model.

Edge Concentration	Value	Interior Concentration	Value
$c^E_{m,ss}$	0.036	$c^I_{m,ss}$	0.033
$c^E_{a,ss}$	0.068	$c^I_{a,ss}$	0.035
$c^E_{p,ss}$	0.165	$c^I_{p,ss}$	0.202
$c_{2,ss}$	12.4		
$c_{f,ss}$	2.19		

Parameter Fitting Procedure

Parameter fitting was done by solving constrained least-square problems utilizing the MATLAB fmincon function. Six parameters in total were fitted, and the remaining parameters were obtained either directly from the literature or from steady-state constraints. Data-fitting was done in two steps. First, parameters involving PLC dynamics (d_{plc} and I_{stim0}) were determined by fitting the solution of Eqn. (7), to the data from Mouneimne et al. (2) (see Fig. 2). We then fit the steady-state fractions R_2 and R_a, and the rate constants d_{hyd} and k_{mp}. Here, the full system (Eqn. (7-17)) was solved at each data-fitting iteration. Two separate data sets were used: (a) the barbed-end measurement reported

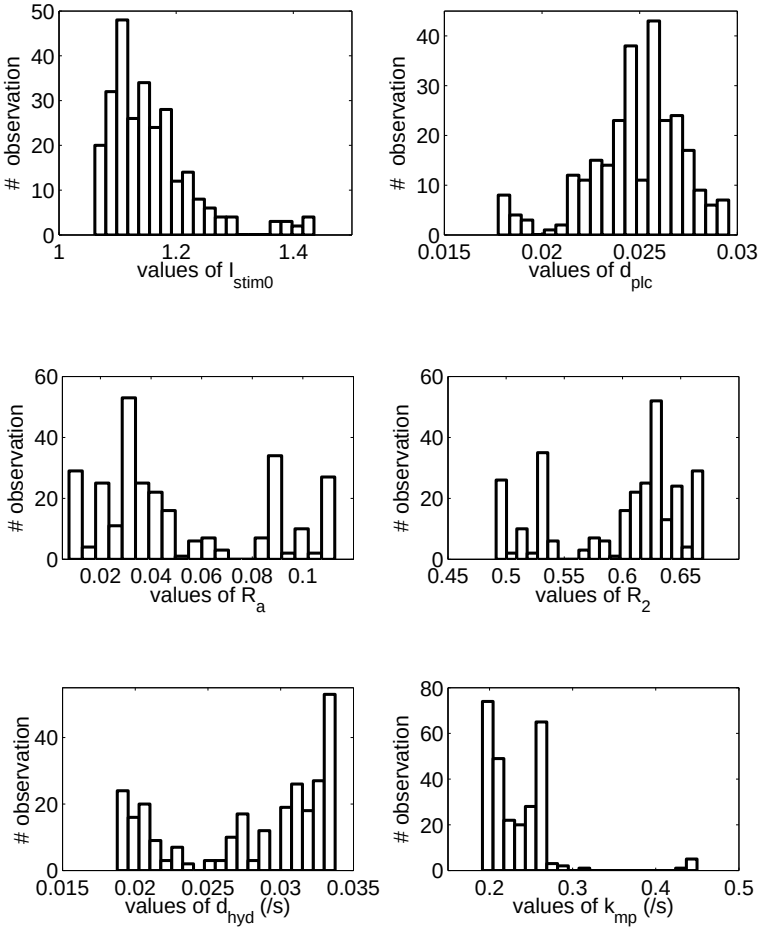

Figure S4: Distribution of parameter values obtained from the bootstrap procedure with 300 data sets. From the PLC data, the distributions for the parameters I_{stim0} and d_{plc} show strongly preferred values. However, the distributions for the remaining parameters are not as sharply peaked. This could be caused by the fact that there are only a small number of data points available for fitting. Nonetheless, simulations done with a set parameter with values that lie within the 95% interval (Table 1 in the paper) yield a result that is qualitatively similar.

in Mouneimne et al. (2) (denoted as (t_i, dat_b^i) with $i = 1, 2, 3$) and (b) the phospho-cofilin level shown in Song et al. (4) ((t_j, dat_{cp}^j), $j = 1, ..., 5$). Note that only the first three time points (first minute following stimulation) of the barbed end data were used as later barbed end level depends on Arp2/3 activity (not currently in our model). We define the sum squared-difference function,

$$G(R_2, R_a, d_{hyd}, k_{mp}) = \sum_{i=1}^{3} (b(t_i) - dat_b^i)^2 + \sum_{j=1}^{5} (c_p(t_j) - dat_{cp}^j)^2, \tag{S37}$$

where $b(t_i)$ is the ODE solution of the barbed end equation at time t_i with the specified parameter input, and $c_p(t_j) = v_E \cdot c_p^E(t_j) + v_I \cdot c_p^I(t_j)$, the whole-cell amount of phosphorylated cofilin at time t_j. This function was then used as an objective function to be minimized. The parameter values were also constrained such that $0 < R_2 < 0.7$, $0 < R_a < 0.1$ and the rate constants d_{hyd} and k_{mp} are positive.

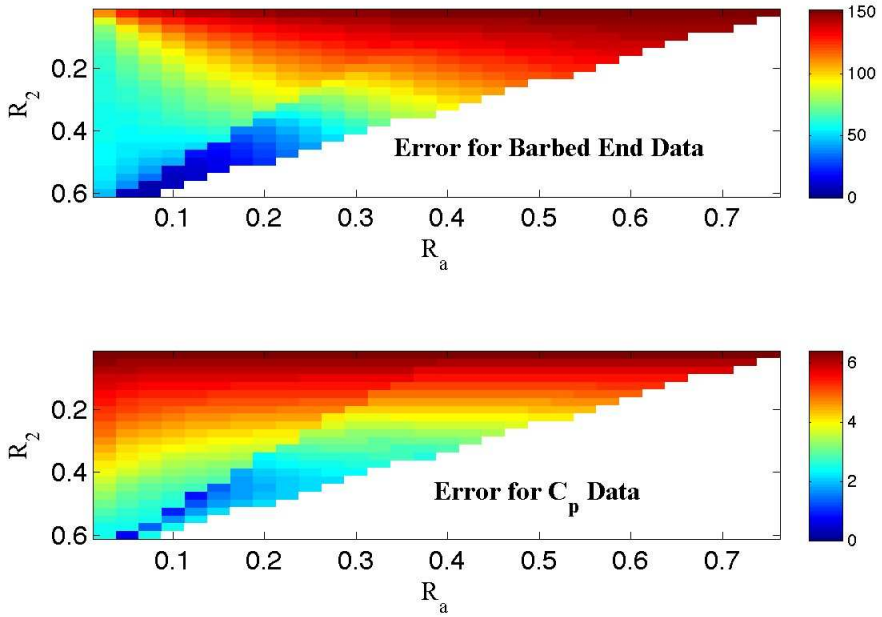

Figure S5: A good fit to barbed end (top panel) and phospho-cofilin (bottom panel) data sets is obtained only if the resting cell has a high level of PIP_2-bound cofilin, i.e. if $R_2 = v_E c_{2,SS}$ is large. Plots of error obtained from fitting d_{hyd} and k_{mp} while varying R_2 and $R_a = v_E c_a^E + v_I c_a^I$. The mean squared differences of simulation and experimental data are shown. Optimal parameters are in dark blue. (The white portion of the panels is inadmissible by conservation).

To measure the quality of data-fitting, a bootstrapping procedure was performed. 300 data sets were generated by sampling with replacement in the original data set. Parameter

fitting was done for each of these data-sets to obtain a distribution of parameter estimates. The 95% confidence intervals computed from the parameter distribution are listed in Table 1 of the article. Histograms indicating parameter distributions are shown in Fig. S4.

Sensitivity to Parameter Values

To ensure that our chosen parameter set is at a global minimum, we looked at the error in the data fits over a broad range of parameter values. Specifically, we performed multiple rounds of data-fitting by varying the steady state fractions R_2 and R_a and fit the rates k_{mp} and d_{hyd} for each (R_2, R_a) pair. The results are shown in Fig. S5. A good fit to both the amplification and the timing of the barbed end peak is obtained only for a large value of R_2 (approximately 50-60%). Values of R_2 and R_a are constrained more strictly by the phospho-cofilin data. There is a narrow range of values of R_2 and R_a that yields a good fit to the data. The final choice of parameter values listed in Table 1 (main paper) lies within the range that yields the minimal difference between simulation result and experimental observation.

5 Comparing the One and Two- Compartment Models

One-Pool Model Equations in Nondimensional Form

$$\frac{dplc}{dt} = d_{plc}(I_{stim}(t) + 1 - plc), \tag{S38}$$

$$\frac{dp_2}{dt} = d_{p_2}(1 - p_2) - d_{hyd}(plc - 1)p_2, \tag{S39}$$

$$\frac{dc_2}{dt} = k'_{p_2}\, p_2 c_p - d_{c_2} c_2 - d_{hyd}(plc - 1)c_2, \tag{S40}$$

$$\frac{dc_a}{dt} = d_{c_2} c_2 + k_{off} c_f - (k'_{on} F)c_a - k_{mp} c_a + k_{pm} c_p + d_{hyd}(plc - 1)c_2, \tag{S41}$$

$$\frac{dc_f}{dt} = (k'_{on} F)c_a - k_{off}\, c_f - k_{sev}\phi_F \left(\frac{c_f}{\phi_F}\right)^n, \tag{S42}$$

$$\frac{dc_m}{dt} = k_{sev}\phi_F \left(\frac{c_f}{\phi_F}\right)^n - k_{mp} c_m + k_{pm} c_p, \tag{S43}$$

$$\frac{dc_p}{dt} = k_{mp}(c_a + c_m) - 2k_{pm} c_p - k'_{p_2}\, p_2 c_p, \tag{S44}$$

$$\frac{db}{dt} = k_{cap}(1 - b) + A\, k_{sev}\phi_F \left(\frac{c_f}{\phi_F}\right)^n. \tag{S45}$$

Note that in this scaled version, each c_i represents a fraction of the total cofilin and $c_2 + c_a + c_f + c_m + c_p = 1$.

To make a correspondence between the models, note that the variables that are restricted to the cell edge in the two-compartment model are assumed to be uniformly distributed in the one-compartment model. This means that certain dilution factors are required to reflect the change of volume in which the reaction is assumed to occur. For example, in

the two-pool model, p_2, is the (non-dimensional) concentration of PIP_2 within the membrane edge compartment. In the one-pool model its (comparatively diluted) level would be $(p_2\, V_E)/V_{tot} = p_2 \cdot v_E$ in the reaction term describing cofilin rebinding to PIP_2 as now the reaction takes place in a larger single-pool. We absorb the volumetric factor in the one-pool rate constants by defining $k'_{p2} = k_{p2}\, v_E$. Similarly, for the term describing F-actin binding, we defined $k'_{on} = k_{on} v_E$.

Table S4: List of parameter values used for the one compartment model. Parameter fitting results and parameter values taken from the literature were used as in the two-compartment model. Parameter values shown in **bold** are used to maintain the same steady-state constraints.

Parameters	Definition	Values
EGF Stimulation		
I_0	Stimulus amplitude	1.14
t_{on}	Time at which EGF stimulus starts	25 s
t_{off}	Time at which EGF stimulus ends	85 s
PLC and PIP_2 Dynamics		
d_{plc}	Basal PLC degradation rate	0.026/s
d_{hyd}	PLC-induced PIP_2 hydrolysis rate	0.032/s
d_{p2}	Basal PIP_2 hydrolysis rate	0.002/s
Steady State Fractions of Cofilin		
R_2	Fraction bound to PIP_2	0.62
R_a	Fraction of free active form	0.04
R_p	Fraction phosphorylated/inactive	0.20
R_f	Fraction bound to F-actin	0.11
R_m	Fraction bound to G-actin	0.03
Cofilin Transition Rates		
d_{c2}	Basal c_2 hydrolysis rate	0.002/s
k_{off}	Unbinding rate from F-actin	0.005/s
$k_{on} F \cdot v_E$	Binding rate to F-actin	**0.02**/s
k_{mp}	Phosphorylation rate	0.186/s
k_{pm}	Dephosphorylation rate	0.03/s
$k_{p2} \cdot v_E$	Binding rate to PIP_2	**0.0047**/s
k_{sev}	Severing rate per cofilin molecule	**0.0012**/s
n	Degree of cooperativity in severing	4
Barbed End		
k_{cap}	Barbed end capping rate	1/s
A	Scaling factor for barbed end generation	**7735**

Comparison of Results: Effects of Localization

We compared the two-compartment model presented in the paper with the one compartment model that lacks the distinction between cell edge and interior. An important outcome of this comparison is the significance of localization (Fig. S6). Using similar parameters in both models, we find that the one-compartment variant significantly underestimates the barbed end peak, and the time course of its rising phase. One reason for this discrepancy is

that in the single compartment model, cofilin released from PIP_2 is quickly phosphorylated, leaving little to bind F-actin (k_{mp} is $\sim$2 orders of magnitude higher than $k_{on}F$). Even if the value of k_{mp} is adjusted in the single-compartment model so that the barbed end amplification is consistent with data (Fig. S7), the timing of the peak is too fast and the rise of phospho-cofilin much too slow relative to data (4). From these results, we conclude that membrane-edge localization of F-actin available for severing is an important factor in the large barbed end amplification in the presence of ongoing cofilin phosphorylation.

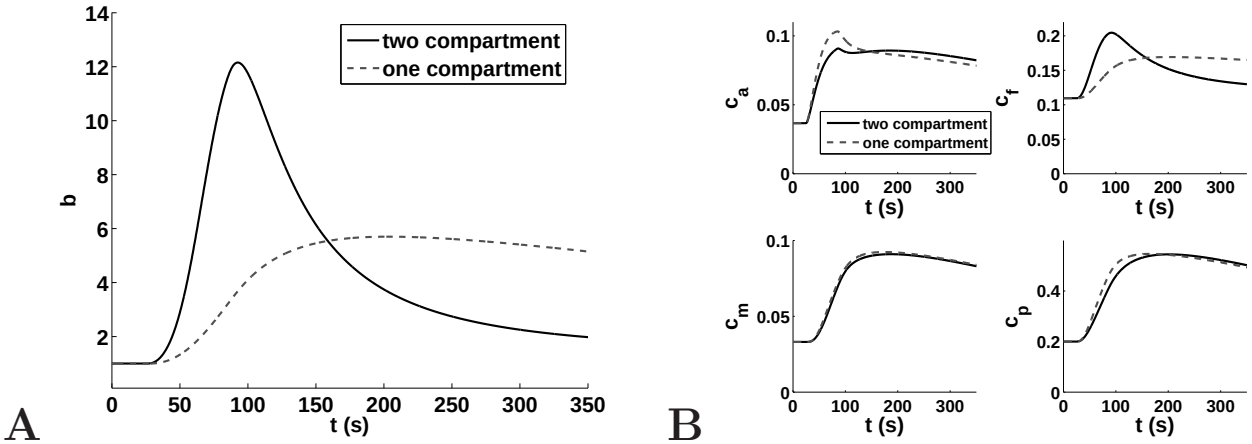

Figure S6: Effect of localization: a comparison of results obtained from the two-compartment model versus one-compartment model. Simulations of (A) barbed ends and (B) cofilin fractions (parameters as in Table 1 in the main paper). Experimental data from Mouneimne et al. (2) and Song et al. (4) (small open dots connected by line segments, shown in red) are shown for comparison.

This localization effect can also be observed by varying size of the membrane edge compartment. In Fig. S8, we show the barbed end profile obtained when v_E is increased from 5% up to 50%. In the latter, the barbed end profile is similar to the one obtained from the one-compartment model. Having a narrow membrane edge compartment allows for targeted and rapid actin binding. As the size of this compartment is increased, the bulk of the released active cofilin is immediately phosphorylated and fewer actin binding/severing events are observed. This is due to the fact that $k'_{on}F = k_{on}F/v_E$ decreases when v_E increases.

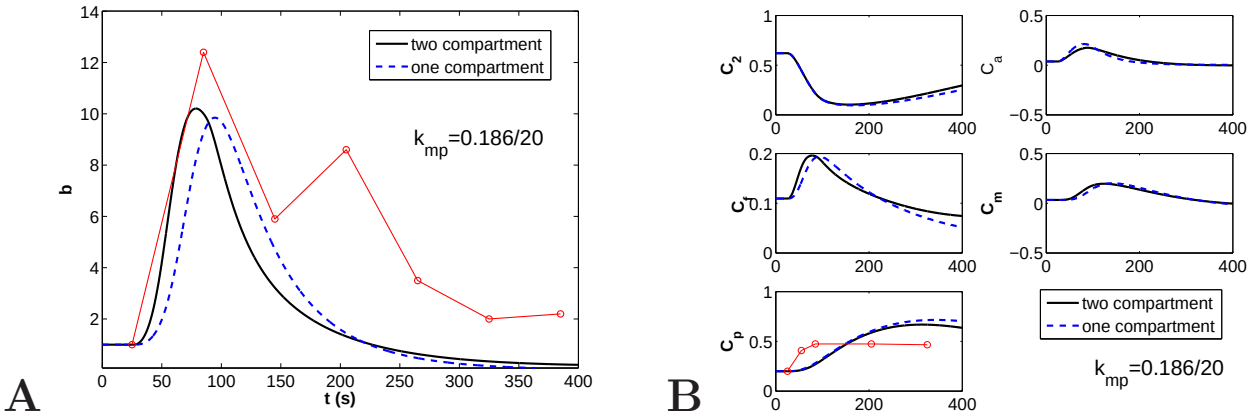

Figure S7: As in Fig. S6 but with a 20 times reduction in phosphorylation rate k_{mp}. (A) Barbed end level and (B) cofilin fractions and experimental data superimposed. In this case, large barbed end amplification is obtained for both models. However, the dynamics occur more rapidly in the two-compartment model than in the basic model. In turn, reducing the value of k_{mp} causes the rise of phosphorylated cofilin to be much too slow compared to observed experimental data.

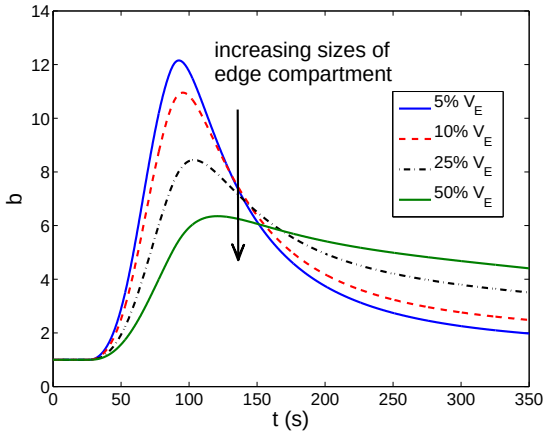

Figure S8: Barbed end profiles obtained from the two compartment model when the relative size of the membrane edge compartment is varied.

6 Results: Additional Figures

The following figures complement the discussion in the main article:

- Fig. S9 shows the dynamics of the nondimensionalized concentrations of cofilin forms in both the edge and interior compartments. Simulations are done under the basic set-up using the the two-compartment model (see Appendix and Table 1) with a 60 s EGF simulation applied at $t = 25$ s. For details, see Results: Basic Behavior section.

- Fig. S10 shows the dynamics of the cofilin fractions when LIMK/SSH is assumed to follow a dynamic increase in activity following simulation. For further description, see Results: Dynamics LIMK section.

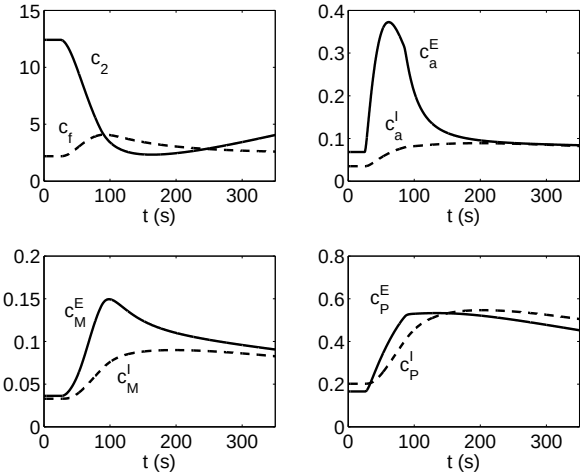

Figure S9: Nondimensional concentrations of cofilin forms (i.e. $c_i = C_i/C_{tot}$ for each i) in the edge and interior compartments. The values of c_2 and c_f are much higher than all other cofilin forms; both species are restricted to the small volume of the edge compartment.

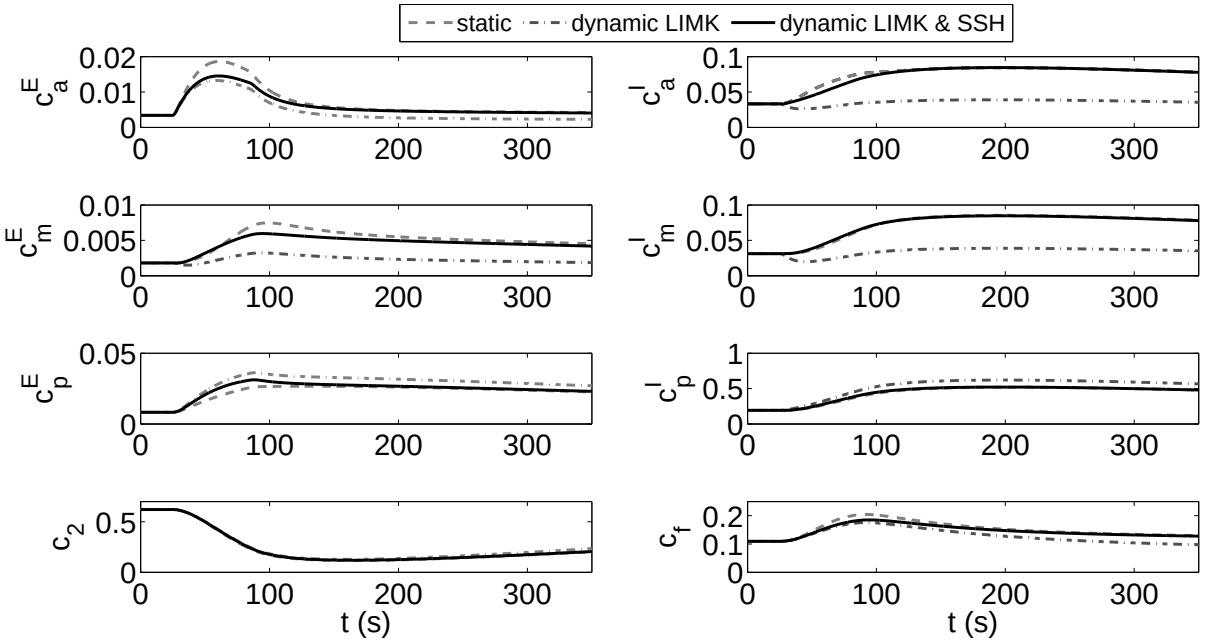

Figure S10: Dynamics of cofilin fractions for the time-varying LIMK and/or SSH.

References

[1] De La Cruz, E. M. 2005. Cofilin Binding to Muscle and Non-muscle Actin Filaments: Isoform-dependent Cooperative Interactions. *J Mol Biol*. 346:557 – 564.

[2] Mouneimne, G., L. Soon, V. DesMarais, M. Sidani, X. Song, S.-C. Yip, M. Ghosh, R. Eddy, J. M. Backer, and J. Condeelis. 2004. Phospholipase C and cofilin are required for carcinoma cell directionality in response to EGF stimulation. *J Cell Biol*. 166:697–708.

[3] Pollard, T. D., L. Blanchoin, and R. D. Mullins. 2000. Molecular mechanisms controlling actin filament dynamics in nonmuscle cells. *Annu Rev Biophys Biomol Struct*. 29:545–76.

[4] Song, X., X. Chen, H. Yamaguchi, G. Mouneimne, J. S. Condeelis, and R. J. Eddy. 2006. Initiation of cofilin activity in response to EGF is uncoupled from cofilin phosphorylation and dephosphorylation in carcinoma cells. *J Cell Sci*. 119:2871–81.